Channel Fading for Mobile Satellite Communications using Spread Spectrum signaling and TDRSS[1]

Jeffrey D. Jenkins, Yiping Fan, and William P. Osborne

Department of Electrical and Computer Engineering
New Mexico State University, Las Cruces, NM 88003

Abstract

This paper will present some preliminary results from a propagation experiment which employed NASA's TDRSS and an 8 MHz chip rate spread spectrum signal. Channel fade statistics were measured and analyzed in 21 representative geographical locations covering urban/suburban, open plain, and forested areas. Cumulative Distribution Functions (CDF's) of 12 individual locations are presented and classified based on location. Representative CDF's from each of these three types of terrain are summarized. These results are discussed, and the fade depths exceeded 10% of the time in three types of environments are tabulated. The spread spectrum fade statistics for tree-lined roads are compared with the Empirical Roadside Shadowing Model.

1. Introduction

Many previous measurements of the mobile satellite channel have used narrow band signaling techniques [1], [2], and have been primarily obtained at UHF, L-Band, and K-Band frequencies. In contrast, this paper will describe an experiment which measured the characteristics of the mobile satellite propagation channel at 2090 MHz using spread-spectrum signaling techniques.

The results from mobile satellite experiments summarized in [3] have confirmed that fades due to shadowing and multipath are significant. To mitigate the fading on such channels, system architects have looked towards spread spectrum signaling. One of the principal advantages of spread spectrum systems is their performance gain against jamming or interfering signals. This is true even when the interference is a multipath component of itself, provided that the time delay of the multipath is longer than one chip time (the chip time being a design parameter of the system). Under such conditions, spread systems should not experience the same degree of fading as unspread systems. It is unknown how much of these gains may be realized in practice since it depends on the distribution of multipath delay spreads.

[1]The authors wish to acknowledge the funding of this research under NASA Grant NAG-5-2142, and for the arrangements which NASA made to permit the use of TDRSS in making these propagation measurements.

Recent work by Ghassemzadeh et al [4] as well as Ikegami et al [5] has been aimed at using spread spectrum measurement apparatus to measure delay spreads in urban and indoor environments. However, no work appearing in the literature has attempted to measure such channel properties in a large number of environments, and no direct comparison of fade statistics for narrow band and spread signaling has been made in typical operating conditions.

The experiment described in this paper utilized NASA's Tracking and Data Relay Satellite System (TDRSS) as a signal source, and measured the channel characteristics with a mobile receiver. This data collection experiment covered 21 representative geographical locations in the Western and Southeastern regions of the United States. For the sake of brevity, Cumulative Distribution Functions (CDF's) for the fading in only 12 of these regions are presented: four each for cities, tree-lined roads, and open areas. Representative CDF's for these three classes of areas are summarized, and the CDF from the tree-lined road areas are compared with a narrow band measurement model. For each of these types of areas, the best case, worst case, and median fade levels observed are tabulated. The sections that follow will describe the experiment in sufficient detail to understand how the propagation data were gathered. Following this description, the basic statistics of the mobile channels will be presented.

2. Experimental Overview

To accomplish the task of measuring channel fade statistics for a spread spectrum communications link, a spread signal was transmitted from geostationary orbit to an instrumented mobile receiver. For this research, the spread signal was uplinked at Ku-Band through the White Sands Ground Terminal (WSGT), to TDRS F3, from which the signal was relayed back to the mobile receiver at S-Band. Figure 1 illustrates the basic concept of the measurement.

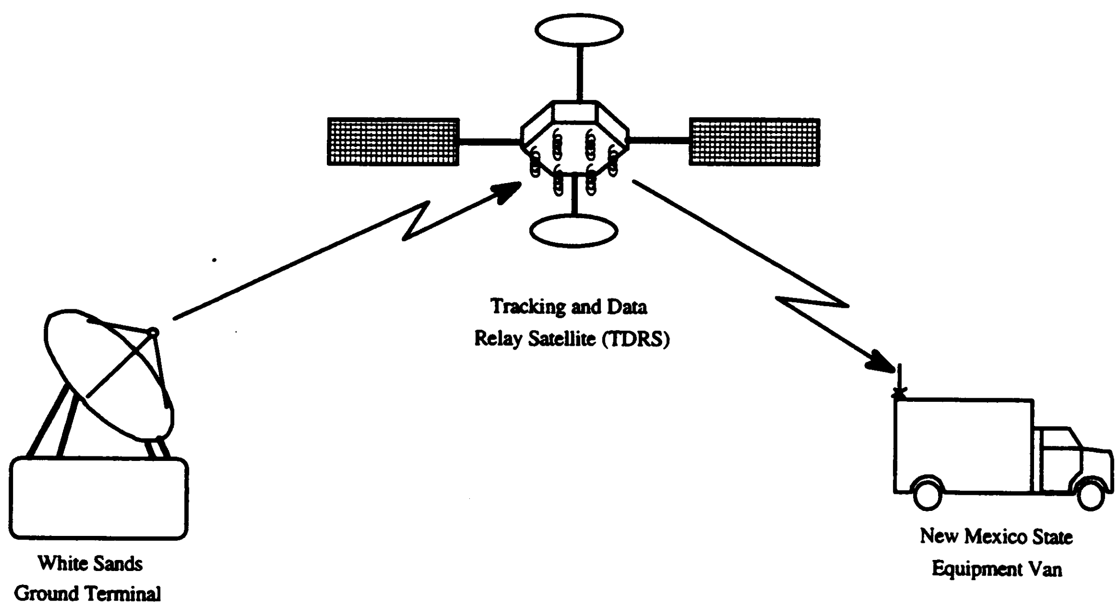

Figure 1. S-Band Test Concept

The performance of the channel was characterized by measuring the energy in the received wave form as the instrumentation was moved through the test areas. The receiver was calibrated against line-of-sight signal levels, providing statistics of the excess path loss due to shadowing and multipath effects. To achieve the goal of developing accurate empirical channel models for a *variety* of environments, it was important to pick appropriate locations in which to collect the data. These locations should be representative both in elevation angle to the satellite, and in topographical features. Using TDRS F3 located at 61° W, the elevation angle contours to the satellite were as shown in Figure 2 below. It can be seen that the elevation angles vary from about 55° in southern Florida, to about 8° in the Olympic Peninsula of Washington.

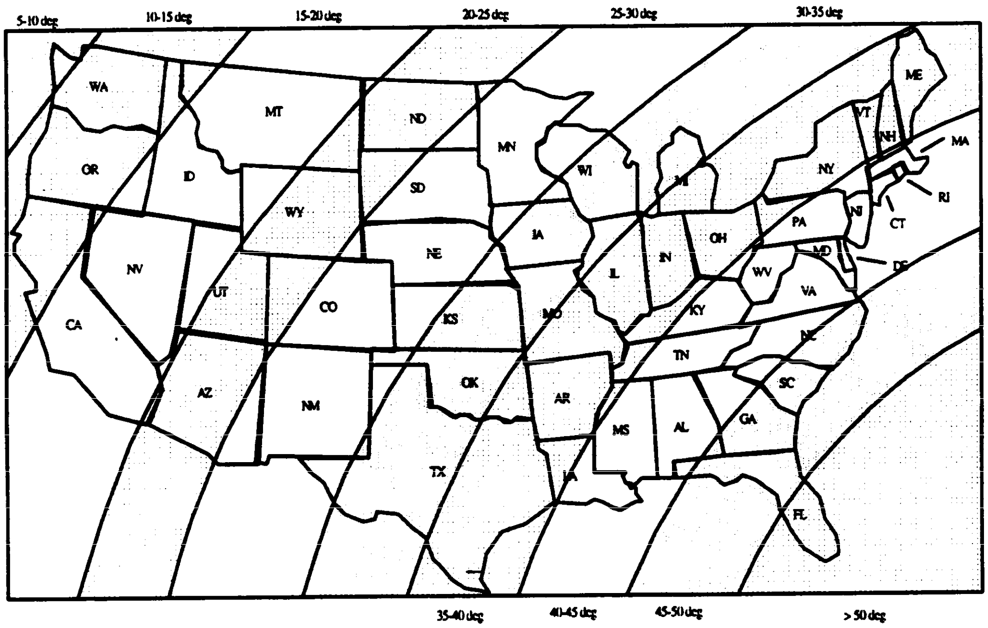

Figure 2. Look Angles to TDRS F3 at 61°W.

The NMSU measurement system was designed around an analog SAW matched filter[2]. The filter was matched to a 1024-bit acquisition sequenced derived from a much longer Gold code. The transmitter located at WSGT continuously transmitted this 1024-bit sequence as it was clocked out at an 8 MHz rate. The resulting BPSK signal, after filtering, occupied nearly 16 MHz of bandwidth. After propagation through the channel, this signal was received, amplified, and down converted for processing through the matched filter. At the output of the envelope detector, a wave form may be observed such as that depicted in Figure 3. There is a large response from the matched filter once per 1024-bit cycle. This response occurs when the pattern of the incoming signal envelope is aligned with the geometry of the SAW device in the filter. The amplitude of the peak response is directly related to the total energy in the 1024-bit symbol.

[2]For complete details of the design, fabrication, and verification of the spread spectrum measurement system, see [6].

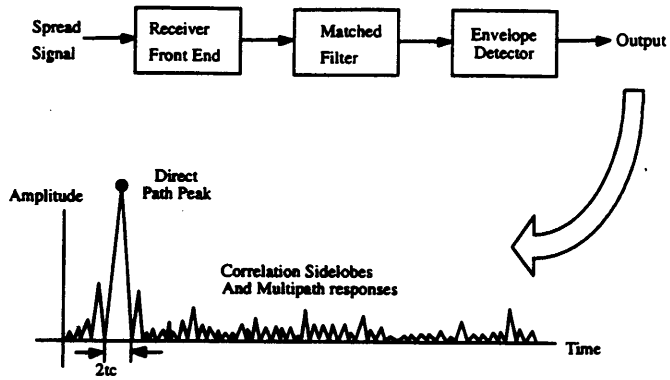

Figure 3. Response at receiver output

The principle of operation of the receiver structure is as follows. If there is no multipath present on the channel, there will be only one response at the output per 1024-bit sequence. If, however, multipath is present, it will appear as a time delayed and attenuated response at the output. Sampling the output of the matched filter provides a measurement of the delay profile for the channel for each sequence repetition, and the amplitude of the largest response in this profile provides statistics on the channel fading that would be observed by a single channel receiver.

The propagation data presented in this paper were collected by sampling the output of the matched filter at a 50 MHz rate. Sampling was not uniform since it was only desired to observe multipath returns from a few miles away. Figure 4 shows the timing of the samples. A receiver circuit synchronized the data collection with the incoming signal, and samples were collected in 20 μs bursts around each peak response. Each burst of data collection provides a measurement of the delay profile of the channel, extending from -2 to +18 μs relative to the direct-path response. With the hardware employed, it was possible to collect 30 delay profiles before pausing the collection to transfer samples to storage. The transfer took approximately 3 seconds, so that 3 second gaps exist in the data collection every 30 profiles.

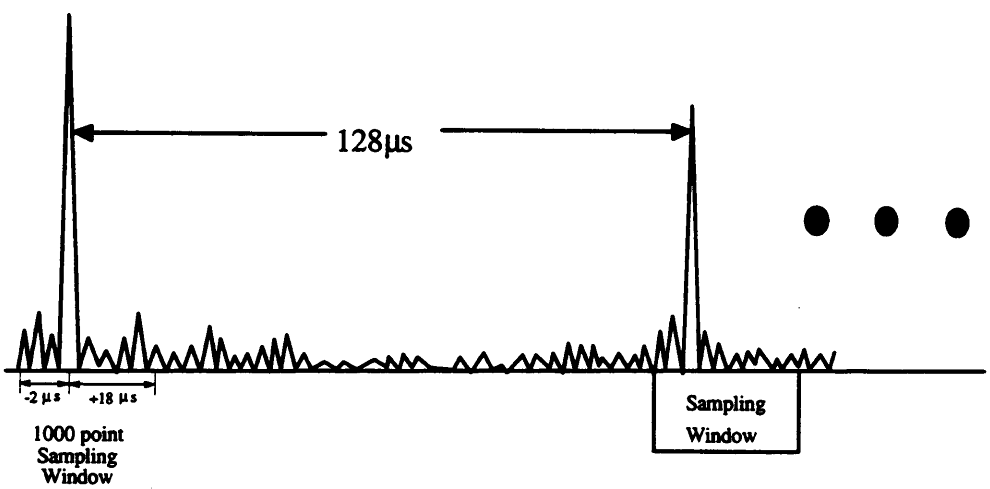

Figure 4. Timing of waveform sampling at the receiver output.

3. Data Collection

Data collection proceeded in two phases. First, the function of the system was verified with a satellite loop-back test. Details pertaining to the system validation testing are given in [6]. Following the equipment check-out, propagation data were collected during two journeys through the United States. The routes were selected to provide measurement opportunities in a variety of environments. Route 1, shown in Figure 5a, passed through the Western US, following a route North from Las Cruces, NM, to Denver, to the Olympic Peninsula of Washington, South to San Francisco, and Eastward back to Las Cruces. Route 2, shown in Figure 5b, encompassed much of the Gulf Coast region of the US, passing from Las Cruces across Texas to Houston along I-10, northward through Mississippi and Arkansas, and finally across the plains of Oklahoma and the Texas Panhandle back to Las Cruces.

Several propagation issues were involved in selecting the test areas. In order to address questions about the performance of spread spectrum systems in multipath environments, it was necessary to collect data in such areas. Geometrical considerations lead to that the conclusion that the delay spread profile in a "city canyon" environment would be quite different from that found in mountainous or real canyon areas. In response to these considerations, sites were selected in several major cities as well as in mountain and canyon areas. Another question addressed by this experiment was to examine how different the fade statistics for spread systems are compared with models developed from CW measurements under shadowing (non-multipath) conditions. This led to the selection of test areas in both heavy and light tree-shadowed environments. Finally, several sites were selected in open areas, where fading was expected to be light. The resulting fade distributions were expected to be identical (in a statistical sense) with similar distributions measured by CW experiments.

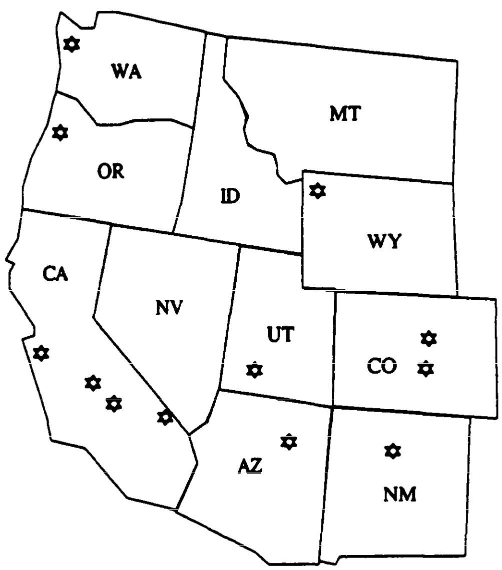

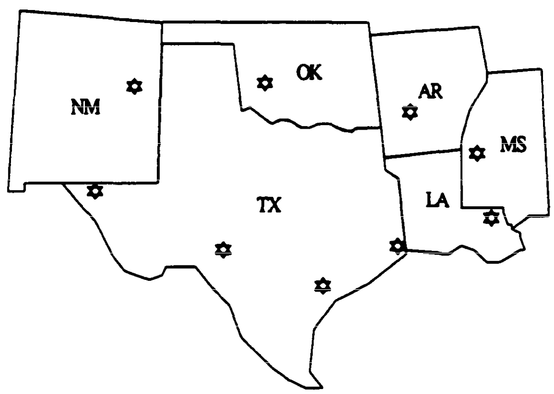

Figure 5. Details of the routes along which data was collected. (a) Western route, and (b) Southeastern route.

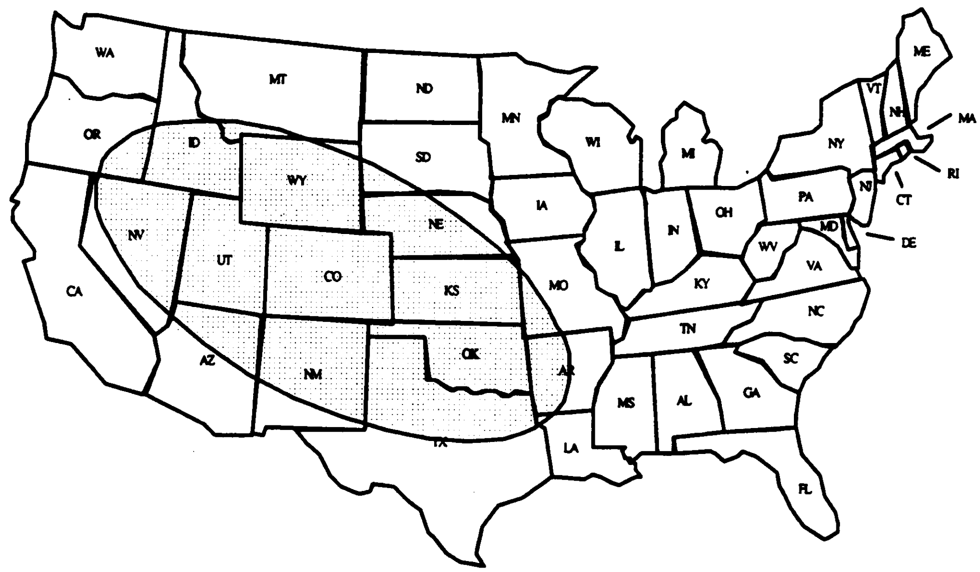

Figure 6. A Typical TDRSS S-Band 3 dB footprint. Shown here with the beam centered on Denver, CO.

In the two figures above, locations with a ✡ represent regions where propagation data was collected. The twelve locations along Route 1 included: Albuquerque; Pikes Peak; Denver; Yellowstone Park; the Olympic Peninsula of Washington; Portland, OR; San Francisco; Yosemite Park; Sequoia Park; the Mojave Desert; Zion Park; and US-180 across Arizona. Tests along Route 2 included: I-10 East of El Paso, TX; I-10 West of San Antonio, TX; I-10 through Houston; Galveston, TX; New Orleans, LA; Vicksburg, MS; Central Arkansas; Central Oklahoma; and Eastern New Mexico. Figure 6 shows how the half power beam width of the TDRSS S-Band antenna compares with the size of the test areas. Under worse case conditions, where the receiver was moved at 65 mph during the three hours of data collection, the expected amplitude change due to movement through the footprint would be less than 0.5 dB. In addition, the Doppler observed on the signal due to the motion of the vehicle was on the order of 200 Hz, which also had no measurable effect on the received signal strength.

4. Fade Distributions

Following the test plan summarized in the previous section, propagation data was collected in each of the locations specified. Approximately 100,000 individual delay profiles were measured at each location. To improve the effective signal-to-noise ratio, wave form averaging was employed. The 100,000 unaveraged delay profiles were processed into about 3000 averaged profiles. The CDF's shown below represent the distribution of fades observed on the amplitude of the strongest return observable within each averaged delay profile. The fade depths are all referenced to unobstructed line-of-sight levels. Given the relatively small number of samples available for statistical analysis, probabilities less than 0.01 are not shown on the graphs.

In Figure 7, several representative fade distribution curves are shown from urban areas. Figure 8 presents fade distributions for areas where unobstructed line-of-sight propagation was predominant. In Figure 9, the distributions from routes along shadowed roads are presented. Finally, Figure 10 shows an overlay of the fade distributions from Figures 7 through 9.

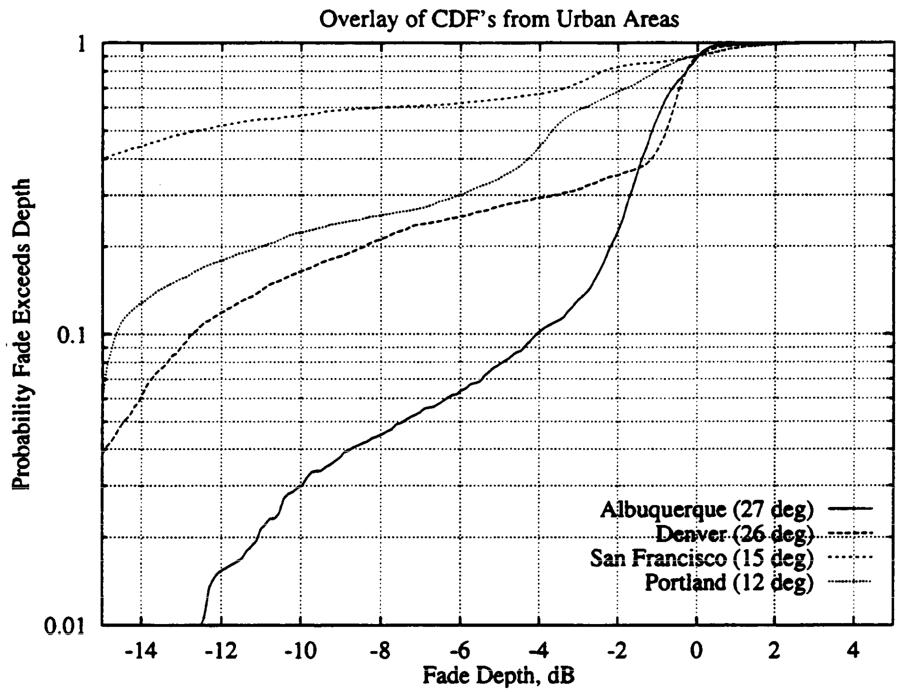

Figure 7. CDF's for Urban Areas

5. Discussion and Conclusions

In the previous section, the fade distributions observed by the S-Band receiver were presented. These curves exhibit two principle slopes. First, in the relatively open areas, the CDF's fall off very rapidly, with very low probability of deep fades. Those fades which do occur are primarily due to ground multipath and atmospheric effects. To see this, one may examine the geometry shown in Figure 11. The height of the mobile antenna is given as h, with the path elevation angle to the satellite given by θ. The differential path length is given as

$$\Delta = (R'+D) - R = R\left(\sqrt{1-4\frac{h^2}{R^2}\cos^2\theta} - 1\right) - \frac{2h\cos^2\theta}{\sin\theta} + \frac{2h}{\sin\theta} \cong 2h\sin\theta \qquad (1)$$

where the approximation holds as h/R goes to zero. This differential path length is less than $2h$ for all elevation angles, or 24 feet in the case of the NMSU experiment. This corresponds to an excess path delay of about 24 ns, which is much less than the chip time of 125 ns. Thus, the multipath is not eliminated by the spread receiver, and can contribute to fades.

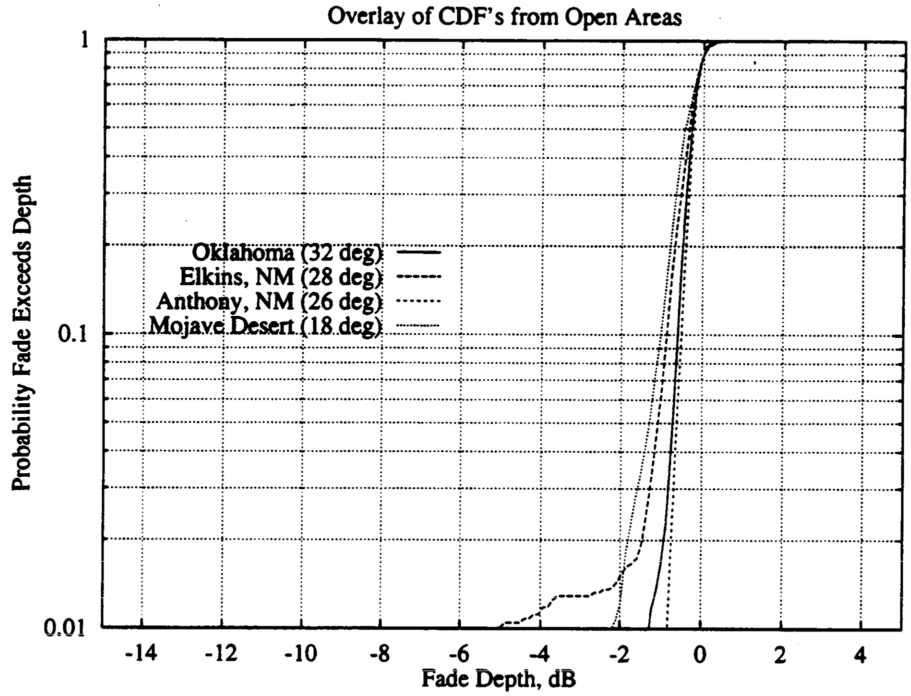

Figure 8. CDF's from Open Areas

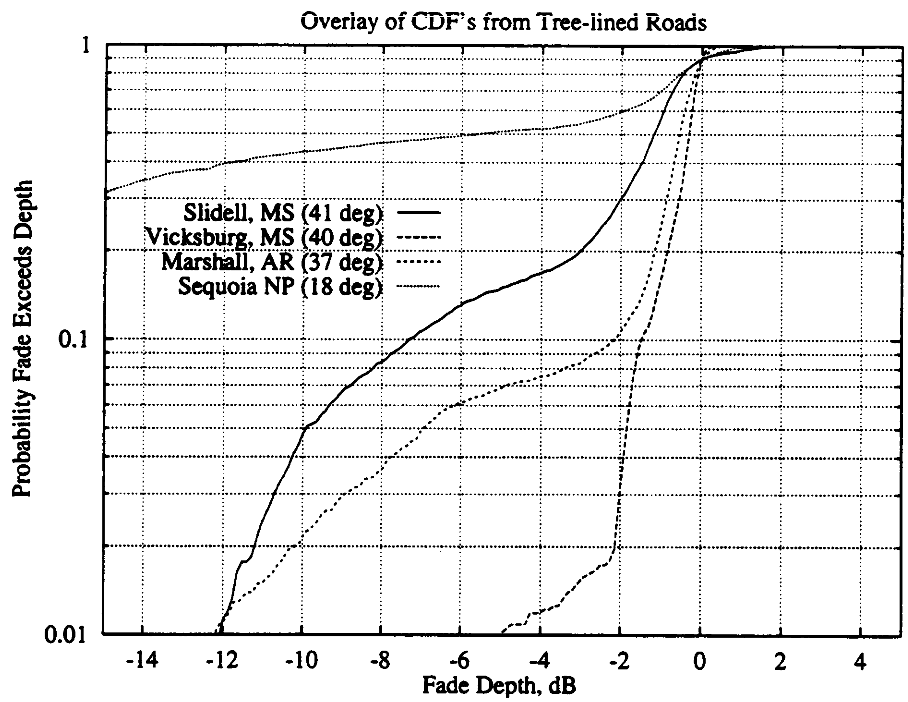

Figure 9. CDF's from Tree-lines Roads

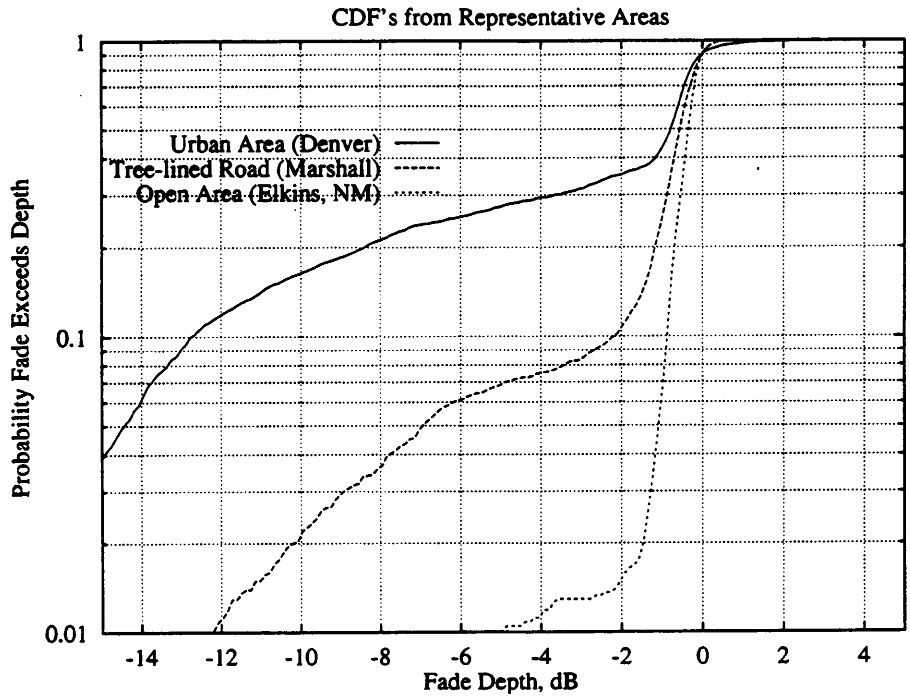

Figure 10. Overlay of the curves from three representative areas.

In the heavily shadowed areas, the CDF's fall off very slowly, with high probability of deep fades. The open areas and shadowed areas comprise the two characteristic slopes for the CDF's. Test areas with a mixture of open and shadowed regions exhibit both slopes, with a knee separating the regions where each effect (shadowing and "flat fading") is dominant.

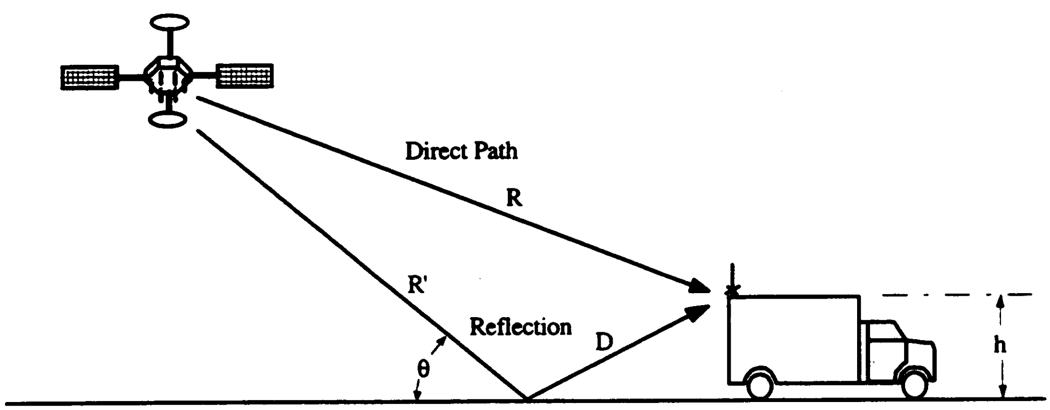

Figure 11. Multipath geometry on flat terrain.

Several statements may be made about the degree to which the fade statistics vary from one type of region to another. Refer to Figure 7, which shows the CDF's in several cities. At the 0.1 probability level, there is a 13 dB separation between the best and worst case fade depths exceeded (the worst case is actually off of the scale of the figure). The curves generally follow a pattern from low elevation angle to high, with the more severe fades occurring in the cities with lower elevation angles. However, it is seen that the fades in Portland (12 degrees elevation) are not as severe as the fades in San Francisco (15 degrees elevation). This demonstrates that not only elevation angle, but also many other features of the city itself determine the severity of the fading that will be observed.

Figure 8 does not hold many surprises. In the open areas, the fade distributions were strictly a function of elevation angle to the satellite. The best case fade distribution was measured in Oklahoma (where the highest elevation angle to TDRS F3 was observed), while the worst case fade distribution was measured in the Mojave Desert (where elevation angles were the lowest).

Figure 9 shows a similar trend in the tree-shadowed environments to that of Figure 7. Generally, the lower the elevation angle to the satellite, the more severe the fades become. The data collected between Slidell, LA, and Bolton, MS appears to have experienced deeper fades than elevation angle alone would account for. Again, the specific type of tree, size of the crown, and spacing between trees are all factors which impact the degree of fading observed.

The performance differences between heavy shadowing (urban), light shadowing (roadside trees), and open areas is clearly evident in Figure 10. The knees in the curves which separate the regions where flat fading and shadowing dominate are also evident. Flat fading is observed in all environments; however, the more sever the shadowing is, the sooner the shadowing effect dominates the fade distribution. In the open area, the knee occurs below the 0.01 probability level and is not observed in the distribution. With light to moderate shadowing, such as along tree-lined roads, the knee occurs at about the 0.1 probability level. Finally, in the urban environment, the knee has moved all the way up to the 0.3 level, and dominates nearly the entire fade distribution curve. The best-case, worst-case, and median fade levels observed during the data collections are summarized in Table 1.

Geographic Area	Best-Case	Median	Worst-Case
Urban Areas	-4 dB	-10 dB	-17 dB
Tree-line Roads	-1.5 dB	-8 dB	-16 dB
Open Areas	-0.5 dB	-0.8 dB	-1.0 dB

Table 1. Summary of fade depths at the 0.1 probability level in three types of environments.

It is interesting to examine how the fade statistics derived from the spread measurements compare with models derived from CW measurements. Using the Empirical Roadside Shadowing Model described in [7], the fade statistics for a mobile system operating in a roadside tree environment at 37° elevation angle were computed. In Figure 12, this curve has been overlaid with the fade statistics from the spread measurements in Central Arkansas. The spread measurement clearly shows the presence of two types of fading - flat fading (multipath from the ground) and shadowing. The knee in the curve marks the transition between the two. The slope of the shadowing portion of the CDF is identical with that of the ERS model, but is shifted to the right. This shift to the right is accounted for because roadside tree shadowing was not present for the entire duration of the data collection.

The knee occurs at a fade depth of between 2 and 3 dB. If the portion of the CDF of interest (between 1% and 20% probability) is extrapolated, and shifted so that the resulting line passes through the origin, then the dashed line in Figure 12 results. The agreement between the ERS model and spread measurement is good. The minor difference in slope is most likely due to differences in the density of the tree canopy. This result indicates that spread systems exhibit the same degree of fading in tree-shadowed environments as do unspread modulation systems.

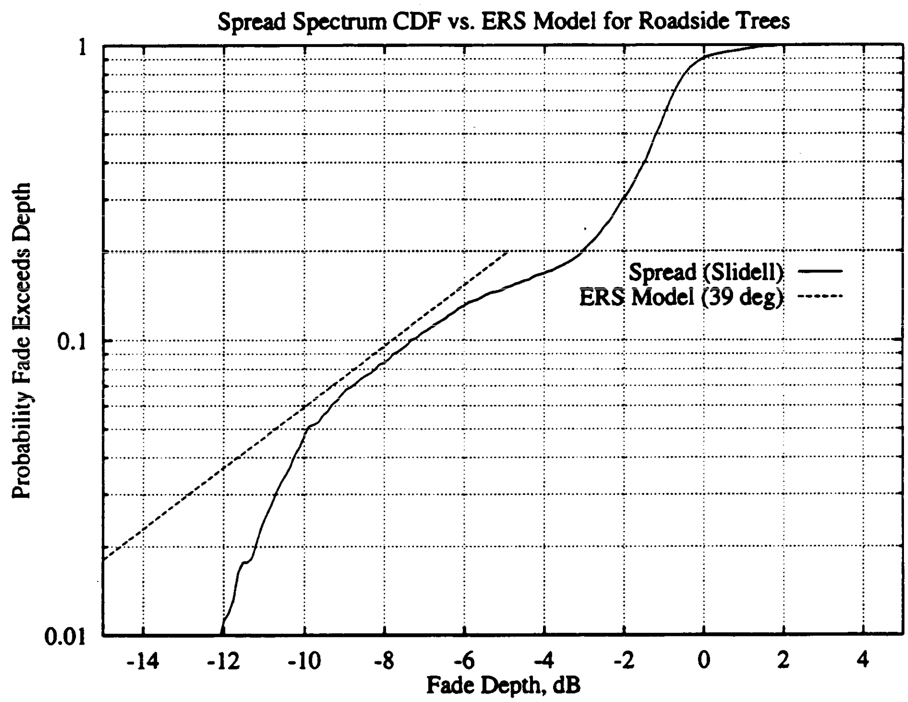

Figure 12. A comparison between the Empirical Roadside Shadowing model and the observed fade distribution at a 37° elevation angle.

Some insight is gained by comparing measurements against models. However, to actually determine the improvement offered by spread signaling in typical operating conditions, it is necessary to collect simultaneous fade statistics with both spread signaling and a CW beacon. Such information will allow the system engineer to determine if there are sufficient gains available from employing spread signaling to justify building such a system for a given operational area. An experiment to simultaneously measure the performance of spread and narrow band systems in the same environments is currently being pursued to address these questions.

References

[1] Vogel, W. and J. Goldhirsh, "Fade measurements at L-Band and UHF in mountainous terrain for land mobile satellite systems," *IEEE Trans. Antennas Propagat.*, vol. AP-36, no. 1, pp. 104-113, Jan. 1988

[2] Goldhirsh, J. and W. Vogel, "Mobile satellite system fade statistics for shadowing and multipath from roadside trees at UHF and L-Band," *IEEE Trans. Antennas Propagat.*, vol. AP-37, no. 4, pp. 489-498, April 1989

[3] Goldhirsh, J. and W. Vogel, "Propagation effects for land mobile satellite systems; overview of experimental and modeling results," NASA Reference Publication 1274, February 1992

[4] Ghassemzadeh, S. et al, "On the statistics of multipath fading using a direct sequence CDMA signal at 2 GHz, in microcellular and indoor environments," *International Journal of Wireless Information Networks*, vol. 1, no. 2, 1994

[5] Ikegami, T. et al, "Field tests of a spread spectrum land mobile satellite communication system," *IEICE Trans. Commun*, vol. E76B, no. 8, August 1993

[6] Jenkins, J., Y. Fan, and W. Osborne, "Wideband propagation measurement system using spread spectrum signaling and TDRS," to appear in the *Proc. NAPEX XIX*, June 1995

[7] Goldhirsh, J. and W. Vogel, "Mobile satellite system propagation measurements at L-Band using MARECS B-2," *IEEE Trans. Antennas Propagat.*, vol. AP-38, no. 2, pp. 259-264, February 1990

Acknowledgment

The authors wish to acknowledge the support of NASA under grant NAG-5-2141 for funding this research and making the TDRSS resources available for the measurements. We also wish to express our gratitude to the many people who worked on fabrication and test of the experimental hardware and the NMSU Engineering Department's mobile experiment van.